Shattered Pellet Penetration in Low and High Energy Plasmas on DIII-D

R. Raman[1], R. Sweeney[2*], R.A. Moyer[3], N.W. Eidietis[4], D. Shiraki[5], J.L. Herfindal[5], J. Sachdev[6], E.M. Hollmann[3], S.C. Jardin[6], L.R. Baylor[5], R. Wilcox[5], T. Carlstrom[4], T. Osborne[4], D. Eldon[4], J.E. Menard[6], R. Lunsford[6], B. Grierson[6]

Email: **raman@aa.washington.edu**
[1]University of Washington, Seattle, WA, USA
[2] ITER Organization, Saint-Paul-Les-Durance, France
[3]University of California San Diego, La Jolla, CA, USA
[4]General Atomics, San Diego, CA, USA
[5]Oak Ridge National Laboratory, Oak Ridge, TN
[6]Princeton Plasma Physics Laboratory, Princeton, NJ, USA

Abstract:

Shattered Pellet Injection (SPI) has been adopted as the baseline disruption mitigation system for ITER, as the radiative payload penetration into DIII-D plasmas from SPI is superior to those using the Massive Gas Injection (MGI) method. Because of the substantial differences in the energy content of ITER plasma and those in present experiments, reliable 3d MHD modeling, benchmarked against present experiments is needed to project to ITER plasmas. In support of these needs, the depth of SPI fragment penetration in DIII-D plasmas was investigated by injecting SPI into two discharges with vastly different energy content and pedestal height. 400 Torr-L pure Ne fragmented pellets at a velocity of about 200 m/s were injected into a 0.2 MJ L-mode discharge and a 2 MJ super H-mode discharge. Results show deep penetration of SPI fragments into low-energy plasmas in DIII-D. SPI fragment penetration is reduced as the plasma energy content increases, with some discharges exhibiting penetration that is confined to the outer regions of the plasma. The injected SPI fragments are also spread out over a distance of about 20 cm, which results in some fragments arriving near the end of or after the thermal quench is over.

* Current affiliation: MIT Plasma Science and Fusion Center, Cambridge, Massachusetts 02139, USA

1.0 Introduction

Early on when experimental work on tokamak plasma disruption mitigation was initiated, solid pellets referred to as 'killer pellets' were employed, which injected a solid low-Z impurity pellet into DIII-D plasma discharges[1]. The emphasis later shifted to high-Z gas injection using fast gas injection[2] valves that rapidly emptied a plenum filled with high-pressure noble gas into the plasma discharge[3]. Much of the Disruption Mitigation studies on many tokamaks is based on this method, which is referred to as Massive Gas Injection (MGI).[4 5 6 7 8] Because of the difficulty in installing these valves close to the ITER plasma (to improve their response time), the excess gas that inevitably arrives after the thermal quench is over would result in a current quench time of less than the allowed 36 ms in ITER,[9] which would induce eddy current stresses on the vessel walls that are higher than the design wall stress limits.[10] Due to the superior results from Shattered Pellet Injection (SPI) experiments on DIII-D,[11 12 13] the disruption mitigation research emphasis on DIII-D has recently shifted to largely studying the capabilities of the SPI system.

SPI is the baseline concept for achieving disruption mitigation on ITER.[14] Thus far, DIII-D is the only tokamak that has extensively reported on disruption mitigation using SPI. It is now also being studied on J-TEXT[15], and a significant amount of JET experiments were completed, but these have not been reported yet.[12] The maximum energy content of a high-power DIII-D plasma used for SPI studies thus far is about 2.2 MJ, which was achieved in the Super H-Mode configuration.[16] This is about two orders of magnitude less than the typical energy content of an ITER discharge which is projected to have stored energy of 350 MJ with central electron temperatures in the range of 14.7 to 27 keV.[17 18] Given the extent of extrapolation that is needed to project to ITER, it is of considerable interest to assess the SPI fragment penetration in DIII-D discharges as the plasma energy content is increased. In addition, extrapolation models require both SPI fragment penetration studies in present tokamaks and supporting 3d MHD modeling that can be reliably benchmarked with data from present experiments.[19 20] In support of these activities, local pellet ablation models are being developed to couple to 3D MHD codes M3D-C1 and NIMROD.[21 22]

In support of these activities, for this first experiment aimed specifically at SPI fragment penetration, SPI fragment penetration was studied in two DIII-D plasmas in which the plasma stored energy content was varied by an order of magnitude. For pellet penetration

into a plasma discharge, the electron temperature and electron density determine the ablation rate of the pellet.[23] The amount of energy contained in the plasma, and the plasma heating (in the radiative payload deposition region) provides a measure of the minimum critical mass of radiative material that needs to be assimilated by the discharge before a rapid cooling of the discharge initiates. For these experiments, 400 Torr.L pure Ne fragmented pellets were injected into a 0.2 MJ L-mode discharge and a 2 MJ Super H-mode discharge. The high-energy target discharge used for the SPI penetration studies was a recently developed Super H-Mode discharge.[16] The stored energy content of these plasma is about twice that of the plasmas previously used for SPI studies on DIII-D.[24]

Section 2 describes the experimental results from this study. In section 3, we describe results from simple 1d simulations that provide an estimate of the depth to which a single SPI-sized fragment could be expected to penetrate in discharges similar to the ones used in this experimental study, and for temperature and density profiles corresponding to those for an ITER-like plasma. Section 4 provides a brief discussion and conclusions from this study.

2.0 Experimental Results

The target discharge used in this study is shown in Fig. 1. The discharge ramps up to 1.6 MA at 1.4 s. Shortly after 1.5 s it transitions into an H-Mode discharge. The electron density and stored plasma energy continue to increase until a peak stored energy of 2.2 MJ is attained. SPI is injected into different phases, of a repeat set of this discharge, to assess the fragment penetration depth as a function of stored plasma energy. The plasma stored energy WMHD in Fig. 1 is obtained from integrating the pressure profile from a plasma equilibrium reconstruction. The three SPI injection times are labeled (*a*, *b*, and *c)* in Fig. 1. Shattered fragments from a 400 Torr-L Ne SPI pellet traveling at a velocity of ~200 m/s were injected (a) during the 0.2 MJ L-mode phase, (b) during the 1.9 MJ H-mode phase, and (c) even later in the super H-mode phase when the plasma energy content reached 2.2 MJ.

Fig. 2 shows the diagnostic layout on DIII-D and the location of the SPI injector used in these studies. SPI fragments are injected from the outboard side of the vessel, from a

location midway between the top and the midplane of the plasma and directed towards the lower inboard region of the DIII-D vessel. Fig. 3 shows the approximate path the SPI fragments would follow inside the DIII-D vessel. The DIII-D SPI-135 injector was used for these studies. It injects pellets from a vertical location corresponding to (R, phi, Z) = (2.15m, 135 deg, 0.57m). The injection location is 0.57m above the vessel midplane and directed down at an angle of 41 degrees. The pellet velocity prior to fragmentation is estimated to be about 200 m/s and it is assumed that the fragments retain this initial velocity. A fast visible camera with a neon line filter (Ne-I), located on the 210-degree port, at the mid-plane port location was used to view the interaction of the SPI fragments with the DIII-D plasma.

2.1 Edge cooling by pre-SPI gas

The first observation from SPI injection in these plasmas was that the propellant gas and vaporized neon (from the SPI fragmentation process) that precedes the solid pellet fragments cools the edge plasma. In both the L-mode and H-mode discharges the plasma edge was significantly cooled by the arrival of the He propellant gas that carried with it Ne gas from the pellet. The Ne gas is presumably entrained with early propellant as Ne is vaporized off the pellet as warm propellant passes over it.

During the L-mode phase, Thomson scattering measurements show a dramatic increase in the edge density as this gas cloud encounters the plasma edge. The resulting cooling effect (shown in the left column of Figure 4) was sufficiently large in the low energy L-mode plasma that it initiated the thermal quench phase. However, the assimilated amount of radiative material was not adequate for a prompt thermal quench. The time at which the thermal quench is over is indicated by a radiative spike much later during the discharge, as discussed later in reference to Fig. 5. The plasma current, however, also begins to decrease (Fig. 5) indicating the start of the current quench phase. For this injection case, the plasma was thus in a slow thermal and current quench phase at the time the solid SPI fragments arrived at the plasma edge. For a representative discharge (No. 172278), the drop in the edge temperature from the target plasma (at t = 1388.04 ms) to the lower level (at t = 1404.13 ms) as a consequence of the cooling induced by the pre-SPI gas is seen in Fig.

4(a). Correspondingly, the edge density increased by several times the initial value due to the accumulation of the pre-SPI ionized gas in the plasma pheriphiry. The third frame of Fig. 4 shows the drop in the electron pressure from the reference target plasma value to the reduced values as a consequence of the cooling by the pre-SPI gas. The plasma stored energy of the reference discharge, prior to SPI injector trigger time, is 0.2 MJ. It drops to 0.13 MJ at the SPI solid fragment arrival time.

The corresponding traces for the Super H-mode plasma are shown in the right column of Fig. 4 for discharge 172281. In this case, the He and neon gas that precedes the solid fragments sufficiently cool the edge so that the edge pedestal is lost. The plasma energy content reduces from the initial 2 MJ to 1.6 MJ and the plasma is degraded from a Super H-mode discharge to a high power L-Mode discharge. The pedestal electron temperature drops from 2 keV to less than 100 eV. The corresponding density increase at the location of the original pedestal is about a factor of three higher, and the edge electron pedestal pressure drops from near 12 kPa to less than 1 kPa. Consequently, the SPI fragments are injected into discharge that is much less energetic than the original super H-mode target and the discharges also do not have the energetic H-mode pedestal through which the fragments would normally have transited.

This would suggest that future installations of SPI should include additional capability to limit the amount of gas that precede the primary SPI fragments, although some gas contribution such as that released during the fragmentation process itself may be difficult to control. Although the pedestal conditions were strongly affected before the arrival of the SPI fragments, the high-energy plasmas remained robust until the thermal quench is triggered by the arrival of the SPI fragments. This still allowed an assessment of the depth to which SPI fragments penetrate in discharges that has about an order of magnitude difference in their energy content.

2.2 Variation in fragment penetration depth

In this experiment, a total of nine discharges were conducted. Four injections were into a low energy L-mode target at 0.2 MJ. Four injections were into a super H-mode target with an energy content of 2 MJ and a single injection into a 2.2 MJ super H-mode target. Figures

5 to 9 show data from injection into the 0.2 MJ L-Mode discharge, two discharge injections into the initial 2 MJ super H-Mode discharge and a final fourth injection into an initial 2.2 MJ super H-mode discharge.

All four injections into the low-power L-mode show similar penetration behavior, so a single representative discharge (shot 172278) is used to represent this case. Of the four injections into the initial 2 MJ super H-mode, three discharges show sufficiently deep penetration of at least some of the fragments, while the remaining one discharge shows much reduced penetration depth. A discharge from the deep penetration cases as well as the reduced penetration case are also shown. During the single injection into the initial 2.2 MJ super H-mode, the pellet broke into two fragments within the injector. This case also exhibited reduced penetration into the plasma. This case is also shown.

Injection into low power L-mode:

Figure 5 shows experimental traces for injection into the low power L-mode phase of the discharge. As previously noted, the effect of the pre-SPI gas is to reduce the energy content of this plasma from the initial 0.2 MJ to 0.13 MJ at the SPI fragment arrival time. Shown on the left of Figure 5, in frame (a), are traces corresponding to the plasma current and line integrated electron density. The reduction in the plasma current starting from 1410 ms is due to the initiation of the current quench phase of the disrupting plasma. Information from the SPI specific diagnostics which shows the SPI trigger time at t=1390 ms, signal associated with the transit of the SPI within the injector microwave cavity, labeled as 'SPI detector', and a photodiode signal that records the first interaction of the solid SPI fragments with the edge DIII-D plasma are shown in frame (b). Frame (c) shows time traces of Ne-VIII and He-II spectroscopic signals. In frame (d) the ECE signal is from a radiometer that measures broadband, covering the full plasma profile in 2nd and 3rd harmonics. As in the present case, the 3rd harmonic doesn't cut off in most cases and therefore provides a good qualitative indicator of the time scale of plasma thermal energy collapse. The intensity of the radiation emitted at the local values of the electron cyclotron frequency and its harmonics, depends on the electron temperature.[25]Thus, a drop in this signal signifies a reduction in the core plasma temperature, as it is the core that radiates

more intensely. On DIII-D it has been found that this measurement provides a good indication of the core plasma cooling, and in most cases the time duration of the thermal quench. During a prompt thermal quench, such as that shown in Fig. 6, the time between when this signal starts to rapidly drop and when it becomes nearly zero (indicated by the time when the fast bolometer chord shows a large spike) is the duration of the thermal quench. The signal dropping all the way down to zero shows that the core temperature has dropped to a very low level. In this discharge, however, while the ECE signal starts to rapidly drop, it does not quite drop to zero, but rather stays elevated until near the time of the large spike in the fast bolometer signal. This implies that the core temperature is still elevated. Thomson scattering measurements (not shown here) show that at t = 1403.08 ms, which is before the sharp drop in the ECE signal (at t = 1405.5 ms), the core electron temperature is over 1 keV. However, at t = 1408.04 ms, which is just after the drop in the ECE signal, the core temperature has reduced, but it is still about 300 eV, signifying that the thermal quench is not over. At about 1418 ms, when a critical mass of impurities has been assimilated by the plasma (from both the pre-SPI gas contribution plus some contribution from the SPI fragments), the core region is fully cooled, signifying the end of the thermal quench. The last frame (e) shows a core fast bolometer signal. Shown on the right are images from a fast camera diagnostic (corresponding to the view shown in Figure 3). Frame (f) at t = 1414.976 ms shows the edge plasma lighting up when the SPI fragments first arrives at the plasma edge. Frame (g) is at a time corresponding to the thermal quench/current quench phase, and frame (h) at t= 1419.299 ms is at a time corresponding to the current quench phase of the discharge. These are for SPI injection into discharge 172278, during the low-power L-mode phase of the discharge. Similar traces and camera images for the two injections into a 2 MJ super H-mode discharge, and for the single injection into the initial 2.2 MJ plasma are shown in Figures 6, 7, and 9.

The current quench times scales for the low energy (Fig. 5) and high energy (Fig. 6) discharges are different. This is because for the high energy case, a prompt and complete thermal quench is initiated by the SPI itself. This results in an adequate amount of radiative material being quickly assimilated by the plasma discharge, resulting in more rapid current quench. For the low energy discharge shown in Fig. 5, an incomplete thermal quench is

initiated by the pre-SPI gas, which then also transitions into a current quench. Not enough radiative material is assimilated by the plasma, which results in slower current quench.

For all cases, the pre-SPI gas composed of neon and helium and entering the vacuum vessel is clearly seen in frame (c). The gas begins to enter the plasma about 10 ms after the SPI system is triggered. The gradual increase in the plasma electron density, which is a consequence of this pre-SPI gas injection is seen in the density signal on frame (a). An additional 15 ms elapses before the SPI fragments arrive at the plasma edge. This is shown by the first increase in the photodiode signal, on frame (b), that is used to observe the interaction of the SPI fragments with the plasma. Thus, the total response time for the SPI-135 system on DIII-D, from trigger time to the fragments making first contact with the edge plasma, for the injection of 400 Torr.L neon SPI pellet is about 25 ms.

Since the plasma current begins to drop appreciably starting at about 1410 ms, while the radiation spike signifying the end of the thermal quench does not occur until 1418 ms, for these low energy L-mode plasmas, the plasma is in a state of slow thermal and current quench at the SPI fragment arrival time. After the SPI fragments arrive (at about 1416 ms) the core fast bolometer signal sharply increases indicating that the remaining energy in the core plasma has also been depleted. The camera images for these low power L-mode discharges show the light emission to always be confined to the edge region until the thermal quench is over. This is a consequence of the pre-SPI gas that does not penetrate very deep even in these low energy plasmas. It is only during the current quench phase of the discharge that deep penetration of the SPI fragments inside the plasma discharge are seen. The fast camera image (h) quite clearly shows distinct solid particles, that are surrounded by an ablating cloud. This time is also consistent with the recorded spike in the SPI photodiode signal and the core bolometer signal. In these low energy plasmas, the fast camera movies also show the SPI fragments contacting the inner wall of the DIII-D vessel, followed by further fragmentation and vaporization of the remaining material. This ablated neon gas cloud then reenters the current quench plasma from the inboard side. The relevant camera images from this movie file are shown in Fig 10.

These L-mode current quench plasmas are quite useful as they show that if the plasma energy content is sufficiently low, SPI fragments can indeed propagate through the entire

DIII-D plasma. Furthermore, they also show that even after passing the entire plasma many of the fragments have still not fully ablated. This is shown by the fragments impacting the center stack and rapidly vaporizing (Fig. 10).

Injection into H-mode plasma:

The H-mode discharges have thermal energy that is an order of magnitude higher than the L-mode discharges, and the propagation of the shard plume is markedly different. Intense radiation is observed in the vicinity of the shards, however, significant radiation from elongated field-aligned structures is also observed. This is likely because the ablated material is rapidly heated by these high energy plasmas, and it streams along the magnetic field lines. While the location of the SPI fragment itself could be related to the penetration depth (Fig. 8), the streaming bands of light from the Ne-I light is believed to be filament spreading due to parallel and poloidal transport (rapid zonal flows) of cold ablated plasma from the pellets, similar to the observation from MGI experiments.[26] These bands of light are seen, quite clearly, in discharge 172270 (Fig. 7) where some fragments penetrated deeper into the plasma discharge, which should have allowed the ablated material to reach higher temperatures.

In Fig. 7, frame (f), which is during the thermal quench portion of the discharge, shows the presence of a pellet fragment deep within the plasma discharge. Fig. 8a shows the same fast camera data at t = 1903.974 ms, at a time near to that of frame (g) in Figure 7, but 45 μs after frame (g) in Figure 7. Overlaid on Fig. 8b is the estimated location of the q=2 surface. Penetration of Ne shards to the q=2 surface at the time of the thermal quench is observed on discharge 172270, as shown in Fig. 8b. The red line shows the trajectory of the shards and the cyan dots along the trajectory are spaced by 10 cm. The camera images later in time (not shown here) during the CQ portion of the discharge show the bright irregularly shaped structure in the image to consists of many shards. The bright structure is located 50-60 cm from the start of the trajectory near the SPI barrel. This red trajectory is then projected in the R-Z plane and superimposed on an equilibrium reconstruction constrained by magnetics and Motional Stark Effect data and performed at a time just prior to the injection. Measuring 50-60 cm from the start of the red trajectory shows that the

shards penetrate to the region between the q=2 and q=3/2 surfaces when the TQ is triggered. Similar penetration depths are observed for three out of the four Super H-mode discharges (but degraded to a 1.6 MJ L-mode) where the pellet did not prematurely break in the barrel. The shallower penetration in the one out of four Super H-mode discharges is not understood.

In disruption mitigation studies using MGI, the q=2 surface is important as the onset of MHD which results in impurity mixing, and consequently the impurity transport to the core, occurs only after the cooling front which originates outside the q=2 surface reaches this boundary. As described in the third paragraph in Section 4, impurity assimilation during MGI is a complicated process. If enough SPI mass can reach the q = 2 surface (because of direct penetration of the fragments to inside the q=2 surface), then the impurity assimilation during SPI should be much superior, as compared to MGI. That these results show that some fragments penetrate to beyond the q=2 surface in these experiments is an important result, and offers an explanation for why SPI on DIII-D is superior to MGI on DIII-D.

It would be quite desirable for the SPI fragments to be deposited near the magnetic axis as that may offer additional advantages, such as the possible suppression of the initiation of runaway electrons. This requires two conditions to be met; (1) a considerable fraction of the initial pellet mass penetrates to the q=2 surface without ablating, and (2) the transit time of the fragments from the q=2 to the magnetic axis is comparable to or shorter than the thermal quench duration. These experiments show that for the low power L-mode case, condition (1) is met, however condition (2) is not. Satisfying the second condition would require a higher injection velocity. As the thermal energy increases, condition (1) is less well satisfied. Thus, as the thermal energy increases, more material is required to satisfy condition (1), and as in the L-mode case, condition (2) requires that the material travels at a higher velocity.

In the low energy 0.13 MJ discharge the fragments penetrate well past the magnetic axis, which is located at R = 1.7 m, and also reach the inboard side of the DIII-D vessel, which is located at R = 1.016 m. That in the high energy discharges the fragments do not propagate as deep as in the low energy 0.13 MJ discharges, shows that on DIII-D as the

energy content is increased by an order of magnitude, a significant reduction in the SPI fragment penetration can be clearly seen. In addition, as previously noted, these injections are into a discharge that has lost its energetic H-mode pedestal and is much more representative of a 1.6 MJ L-mode discharge.

For discharge 172281 (Fig. 6) which was for injection into an identical H-mode discharge the bands of light are localized much more towards the plasma edge (frames f and g) suggesting much shallower penetration. For this same discharge one also notices much more enhanced emission near the edge (frame g) about 1 ms after the initial SPI fragments arrive (frame f). For fragments traveling at a velocity of 200 m/s this means that the fragments must be spread out over at least 20 cm in length. For this discharge, the light emission in the edge region continues to persist in frame (h) more than 2 ms after the arrival of the first fragments indicating that fragments or ablated neon gas are still arriving 2 ms after the fragments make first contact with the plasma edge. These are also largely consistent with off-line measurements conducted by ORNL. In a recent publication,[12] measurements of shattered argon pellets show that the duration of fragments exiting the shatter tube is < 2 ms with the vast majority within 1 ms. Similar spray durations and fragmentation in between that of D_2 and argon were also observed for neon shattered pellets.

Thus, it must be the vanguard fragments that contribute to the thermal quench and one cannot determine from these studies the actual mass of neon that was responsible for initiating the thermal quench, but it may be much less than the neon inventory in the 400 Torr.L pellet. This behavior is also more clearly seen in frame (h) of Fig. 7, which shows discrete particles inside a current quench phase of the plasma discharge, again showing consistency with the low energy current quench plasma in Fig. 5.

Old experiments on DIII-D found that as little as 10 Torr-L of a neon pellet was adequate to cause a TQ in lower energy plasmas.[27] More detailed measurements that study the minimum required mass of a neon SPI for inducing a TQ as the energy content of the target discharge is varied, in combination with 3d MHD modeling, may be beneficial and necessary for extrapolating this method to high power ITER discharges.

In Fig. 9 (discharge 172286), which was for the case of injection into the initial 2.2 MJ plasma, the fragment penetration is even shallower. On this particular discharge, the pellet broke into two nearly same-sized fragments within the SPI injector. Frame (f) during the thermal quench quite clearly shows the emission to be localized to the plasma edge. The absence of distinct pellet fragments (for example as on shot 172270 in Fig. 7 and Fig. 8) means that these fragments have not reached a region of plasma that has a very high temperature. While the length of the toroidal band could be related to the plasma temperature as a higher temperature plasma could be expected to heat the ablated neon to higher temperatures causing them to move farther away from the ablation region during the time it takes for the fragments to penetrate, interpretation of the significance of the bands of light is much more difficult as a higher temperature plasma will also tend to cause a shorter region of neutral line emission because of faster ionization. Thus, the length of the ablation plume alone cannot be directly related to the background plasma temperature. The broken pellet can be seen in frame (b) of Fig. 9 which shows two distinct spikes for the SPI detector signal. The amplitude of this signal is proportional to the pellet mass so that both broken fragments are approximately equally sized. Frame (g) shows the arrival of a large fragment near the end of the thermal quench, which is likely the second pellet fragment. Apparently, the shatter plume from the first pellet fragment was not sufficient to penetrate deep into these plasmas. This discharge also shows continued edge emission during the current quench phase suggesting fragments are still entering the plasma more than 1.5 ms after the end of the thermal quench.

3.0 1d Simulations of pellet penetration

To gain some insight into these experimental results, numerical simulations were performed to calculate the depth to which a single SPI-fragment-sized pellet could propagate in these plasmas before being fully ablated.

We note here that these calculations do not include the collective effects of the injection of many fragments simultaneously. With the injection of many fragments, the vanguard pellets would cool the plasma, making it easier for the trailing pellets to penetrate deeper.

In these simulations, the electron density and temperature profiles are held constant and the ability of a single 1 mm and 2 mm spherical neon pellet to propagate through this plasma calculated. Because of the very large differences in the edge plasma parameters for ITER and DIII-D, as well as the total stored energy content of these two plasmas, the simple simulations do provide insight into the challenges for pellet penetration that could be expected as the plasma energy content is substantially increased. Modeling using the NIMROD and M3D-C1[20] codes, as well as JOREK[28] that examines the collective effects of SPI-like injection is work in progress.

The pellet penetration code used here was originally developed by Houlberg et al., of ORNL,[29] and includes several ablation models. The neon pellet ablation model of Kuteev[23] was used for these studies. In the Kuteev model, the pellet ablation rate is given by the relation:

$$\frac{dN}{dt} = \alpha n_e^{1/3} T_e^{5/3} r_p^{4/3} M_i^{-1/3} \qquad (1)$$

Here, the term on the left-hand side is the ablation rate of neon in the pellet, n_e is plasma electron density, T_e is the plasma electron temperature, r_p is the instantaneous radius of the pellet, M_i is the grams per mole for the pellet species, and α is Kuteev's ablation rate coefficient for frozen neon.

The code solves for the ablation rate of a pellet injected into a magnetic confinement fusion plasma and determines the pellet radius as the function of distance traveled into the plasma. The radius of the pellet is calculated along the injection trajectory by subtracting out the amount of neon that has ablated from the pellet surface.

In each simulation, a single 2 mm or 1 mm pellet is injected at the SPI injector coordinates corresponding to (R, phi, Z) = (2.15m, 0 deg, 0.57m) at 200 m/s directed down at an angle of 41 degrees. This velocity is consistent with the velocity of unfragmented neon SPI pellets and is consistent with an upper velocity limit for the SPI fragments.

While the size of neon SPI fragments has not been characterized, results from fragmentation tests conducted by ORNL on Argon and deuterium pellets is used to estimate the size of neon fragments. Argon is more difficult to fragment and the velocity of the Ar

pellets used in the fragmentation test was less than the velocity of the neon pellets used in the experiments reported in this paper. The deuterium pellets being less massive have a faster velocity of 400 m/s and shatter into smaller sizes than the Ar pellet. One can reasonably assume that the size of the fragmented neon pellet would be in the range bounded by the Argon and deuterium pellet fragments. Fragmentation tests by ORNL[30 12] of Ar pellet with an initial velocity of 156 m/s and a mass 1.18 g, indicate that 51% of the fragments (by number) have a diameter less than 1 mm, 23% of the fragments have a diameter in the range of 1 to 2 mm, and the remaining fragments are larger in size. For 16 mm sized deuterium pellets, the fragmentation leads to much smaller fragment sizes. 67% of the fragments have a diameter less than 1 mm, 29% have a diameter in the range of 1 to 2 mm, and the rest are larger in size than this.

In the simulations conducted here, it is assumed that a single neon fragment has a diameter of 2 mm or 1 mm and a fragment velocity of 200 m/s.

A pellet with these parameters is injected into plasma corresponding to a 0.2 MJ L-mode discharge and a 1.6 MJ L-mode discharge. The profiles at t = 1388.04 ms, which is before the arrival of the pre-SPI, gas is used for the L-mode case because of the strong cooling and the subsequent initiation of the thermal quench by the pre-SPI gas that does not permit reliable EFIT reconstructions. Thus, for the low-power simulations, one could expect the fragment to penetrate deeper than what is indicated by these calculations.

The electron temperature and density profiles shown in Fig. 4, but smoothed to remove the sharp discontinuities, are used in these simulations. These profiles are shown by the purple and orange traces in Fig. 11a, along with traces for the pellet radius as it propagates through the discharge (blue trace) and the time taken to travel through the plasma (green trace). The electron temperature and electron density information from the Thomson laser that fired at these specific times are only available up to a radius of R ~1.8 m. For the purpose of these calculations, it is assumed that these values remain constant for R < 1.8 m. This assumption is adequate as the calculations indicate that for the high power cases, the pellet is fully ablated by the time it reaches R ~1.8 m. For the L-mode cases, because the Thomson profiles at the time of SPI injection are not reliable, and profiles corresponding to a time well before the SPI injection times are used, the electron temperature is overestimated.

Nevertheless, very deep pellet penetration is seen even for this overestimated temperature implying that under the actual injection conditions the penetration would be even deeper.

For the low energy L-mode case it is seen that the pellet penetrates beyond the magnetic axis (located at R = 1.7 m) of the discharge, and as noted before even deeper penetration would be expected if the post-SPI gas conditions are used. For the1.6 MJ L-mode case (Fig. 11b) on the other hand, the 2 mm diameter pellet penetrates to the q=2 surface. This is somewhat similar to the deeper pellet penetration seen in three of the five injections into the higher energy plasma (for example, discharges 172270 and 172282, with the data from discharge 172270 shown in Fig. 7). These simulations would suggest that these two discharges may have had a larger vanguard fragment size after pellet fragmentation that allowed for the observed deeper penetration, as simulations with 1 mm sized pellet shows much reduced penetration. Alternatively, since the SPI injects many fragments edge plasma cooling by the vanguard fragments may have allowed more of the trailing fragments to penetrate deeper. These results based on present pellet ablation models would suggest that for higher energy plasmas, larger pellets may be warranted as it will lead to larger shattered fragments (for a given speed) and therefore deeper penetration. These questions can be answered by detailed 3d MHD modeling that studies the effect of many fragments being injected at the same time. However, these simulations do clearly show that single shard penetration is strongly affected by an order of magnitude increase in the energy content of even DIII-D sized target plasmas.

To have an idea of how deep these pellets could penetrate in high power ITER plasma, simulations were also conducted for penetration into ITER-like profiles representative of a 350 MJ, 15 MA ITER H-Mode discharge. For the ITER cases, the injection was assumed to be purely radial and from the device mid-plane location as this too would result in the deepest possible penetration. The ITER discharge profiles were obtained from ASTRA simulations carried out by Polevoi.[31] The results shown in Fig. 11c indicates that neither of the two shards is able to reach the q = 2 surface. The much higher edge temperature and density of the ITER plasma causes these small, low velocity pellets to ablate very near the plasma periphery. Again, while the dramatic reduction in pellet penetration with energetic

edge plasma parameters is seen, the impact of injecting numerous pellets simultaneously into larger, more energetic plasmas, combined with reliable 3d MHD modeling[28] [32](that is validated by experimental studies) is required to reliably project to ITER-class plasmas.

It should be noted that the ORNL laboratory studies have shown that as the initial SPI mass increases, the maximum attainable velocity of the pellet decreases.[30] The 200 m/s velocities used in these studies may be an upper limit for the current SPI system being deployed on ITER. The overall response time of the SPI-135 system on DIII-D is 25 ms. Because of the much larger radius of the ITER vacuum vessel and due to difficulties in installing systems close to the plasma, the response time on ITER, of the current baseline system, would probably be slower.

What is also noteworthy is that at a velocity of 200 m/s, about two ms is required for the pellet to travel through the plasma and reach the q = 2 surface on ITER, which is located about 40 cm from the plasma edge. If the vanguard fragments were to initiate a thermal quench, as on the DIII-D experiment, this could result in insufficient pellet material assimilation by the ITER plasma. Simulation results for the DIII-D cases show that for the low-power L-mode case, a single shard easily penetrates to the q = 2 surface, but for the higher power discharge, much of it is ablated by the time it reaches the q = 2 surface.

A dramatic difference in the penetration behavior of a single pellet in these simulations is seen even in DIII-D plasmas as the stored plasma energy content is increased one order of magnitude (i.e. from 0.13 to 1.6 MJ). A similar trend with energy in penetration behavior is also seen experimentally on DIII-D when many shards are injected using SPI. Considering that the ITER 350 MJ plasma has over two orders of magnitude more energy than the highest energy Super H-Mode discharges on DIII-D, and that the q = 2 surface is located twice as far away from the plasma edge than on DIII-D, it would seem prudent that the disruption mitigation system for ITER should strive for ways to increases the attainable velocity of the radiative payload and decrease the overall response time of the system.

4.0 Conclusions

The depth of SPI fragment penetration in DIII-D plasmas was investigated by injecting SPI into two discharges with vastly different energy content and pedestal height. 400 Torr-L pure Ne fragmented pellets at a velocity of about 200 m/s were injected into a 0.2 MJ L-mode discharge and a 2 MJ super H-mode discharge. While SPI fragment penetration very deep into the plasma in low power L-modes is clearly observed, the SPI fragment penetration in higher power plasma is much reduced, but some fragments do reach the q = 2 surface.

Supporting 1d simulations that examined the penetration capability of single 2 mm and 1 mm diameter neon pellet into DIII-D like plasma discharges are qualitatively consistent with the experimental observations. However, these calculations do not include the collective effects of the injection of many fragments simultaneously, but they do provide insight into the challenges for pellet penetration that could be expected as the plasma energy content is substantially increased in ITER-sized plasmas.

In purely MGI mitigated discharges, the injected impurities strongly cool the boundary plasma, near the pedestal. Progressive cooling produces an unstable current profile with evolving and growing islands. Eventually, the cooling and island growth at the q = 2 surface finally triggers rapid cooling of the entire plasma through convection and impurity mixing.[33 34] As well described in the paper by Leonov et al.[10] in simulations examining the impurity gas assimilation by the JET plasma, MGI gas assimilation is a complicated process, not just determined by the gas flow velocity or the proximity of the gas injector to the plasma but one that may be influenced by the plasma response itself.[10] The simulation results show that the energy loss during MGI-initiated disruption mitigation takes place in two phases. The first is the pre–thermal quench (pre-TQ) phase that lasts from the arrival of the first gas to the onset of increased transport due to magnetohydrodynamic activity. This is followed by the second phase (the thermal quench), when most of the energy is radiated. The TQ begins after a critical fraction of impurities is assimilated during the pre-TQ phase so that when the impurity content reaches an amount sufficient for radiative energy loss to overpower joule heating, the cooling front begins to propagate inward accompanied by the plasma current contraction.

These experimental observations on DIII-D and simple 1d calculations suggest that the much superior capability of SPI on DIII-D (compared to MGI) may be due to some fragments penetrating to the q=2 surface, which makes it much easier for a critical mass of impurities to be assimilated by the target plasma. If so, in order to reliably extrapolate to ITER, experiments may need to be conducted in a parameter regime that injects much smaller SPI pellets to result in pellet fragment ablation well outside the q=2 surface, such as what may happen on ITER. A series of SPI mitigated experiments are planned on JET during 2019 and 2020. Given the much larger cross-section of the JET plasma, high energy discharges on JET with energetic H-mode pedestals would be a good target for such experiments aimed at scaling SPI studies for ITER.

Since ITER's discharges that would have more than two orders of magnitude increase in stored energy (over DIII-D plasmas), the need for higher velocity Ne pellets, and or larger fragments, with a faster system response time for deeper penetration should be given serious consideration.

AcknowledgmentsThis material is based upon work supported by the U.S. Department of Energy, Office of Science, Office of Fusion Energy Sciences, using the DIII-D National Fusion Facility, a DOE Office of Science user facility, under Awards DE-FC02-04ER54698, DE-AC02-09CH11466, DE-FG02-99ER54519 AM08, and DE-SC0006757.
Disclaimer: Work supported by the U.S. DOE under Contract No. DE-AC02-09CH11466 with Princeton University. All U.S. activities are managed by the U.S. ITER Project Office, hosted by Oak Ridge National Laboratory with partner labs Princeton Plasma Physics Laboratory and Savannah River National Laboratory. The project is being accomplished through a collaboration of DOE Laboratories, universities and industry. The views and opinions expressed herein do not necessarily reflect those of the ITER Organization. This report was prepared as an account of work sponsored by an agency of the United States Government. Neither the United States Government nor any agency thereof, nor any of their employees, makes any warranty, express or implied, or assumes any legal liability or responsibility for the accuracy, completeness, or usefulness of any information, apparatus, product, or process disclosed, or represents that its use would not infringe privately owned rights. Reference herein to any specific commercial product, process, or service by trade name, trademark, manufacturer, or otherwise does not necessarily constitute or imply its endorsement, recommendation, or favoring by the United States Government or any agency thereof. The views and opinions of authors expressed herein do not necessarily state or reflect those of the United States Government or any agency thereof. DIII-D data showni n this paper can be obtained in digital format by following the links at https://fusion.gat.com/global/D3D_DMP .

Figures

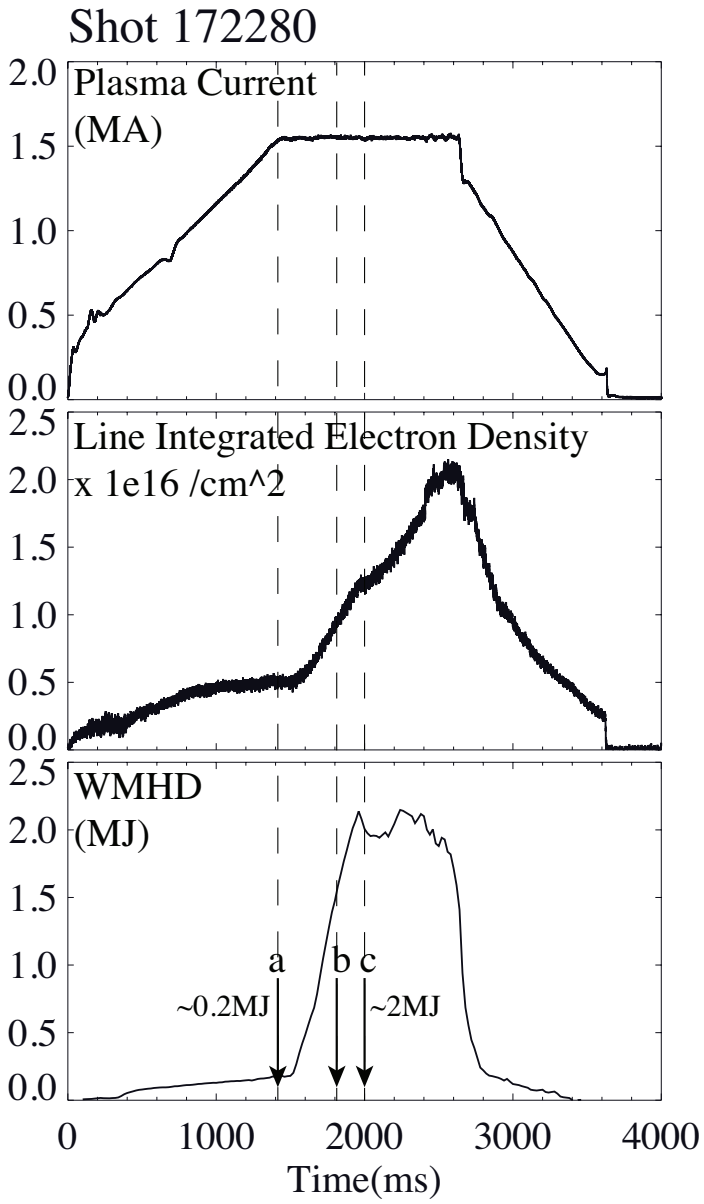

Figure 1: Target discharge used in the SPI penetration study was a recently developed super H-Mode discharge. Shown are from (top) the plasma current, (middle) line integrated electron density, (bottom) the plasma stored energy. SPI injections are carried out at times corresponding to labels a, b, and c in the bottom frame.

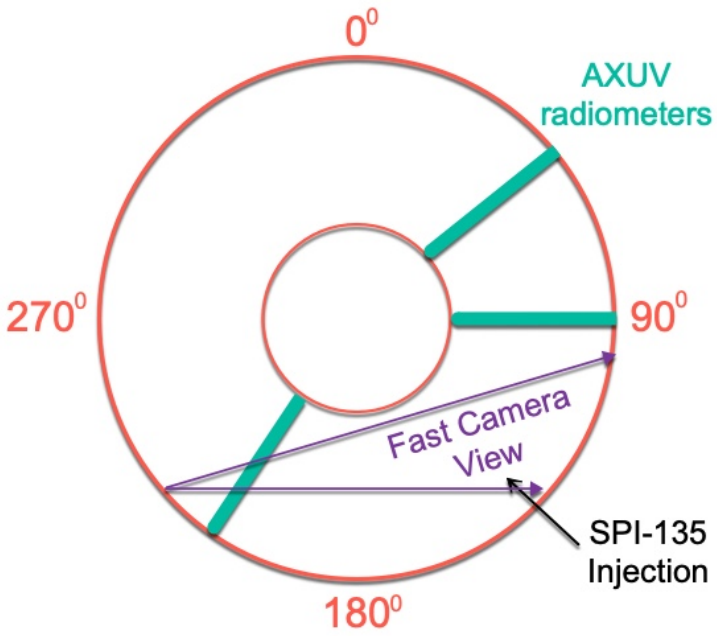

Figure 2: Top down view showing the location of the SPI-135 injector, the fast camera view and the AXUV radiometers

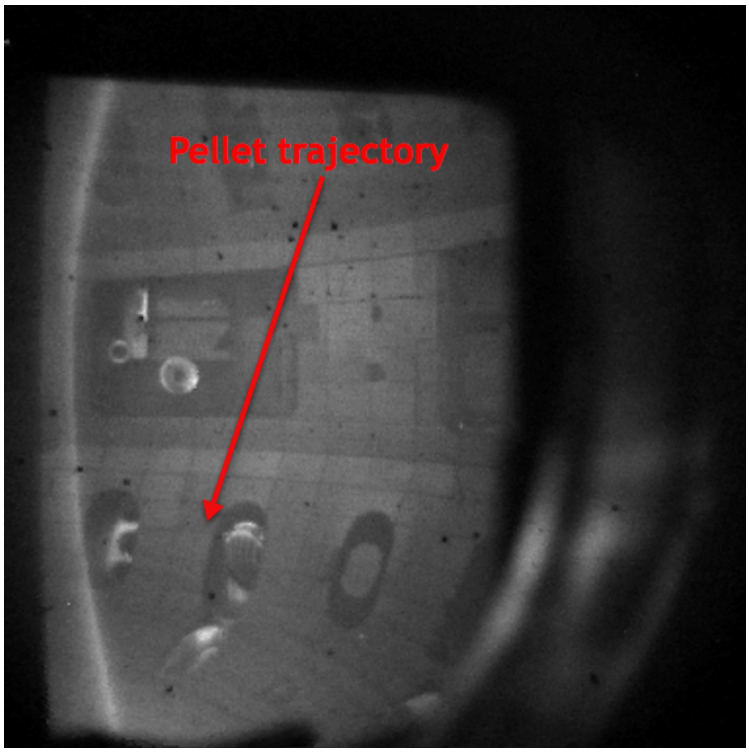

Figure 3: Poloidal view inside the vessel. The red arrow shows the approximate path the SPI fragments would follow inside the DIII-D vessel.

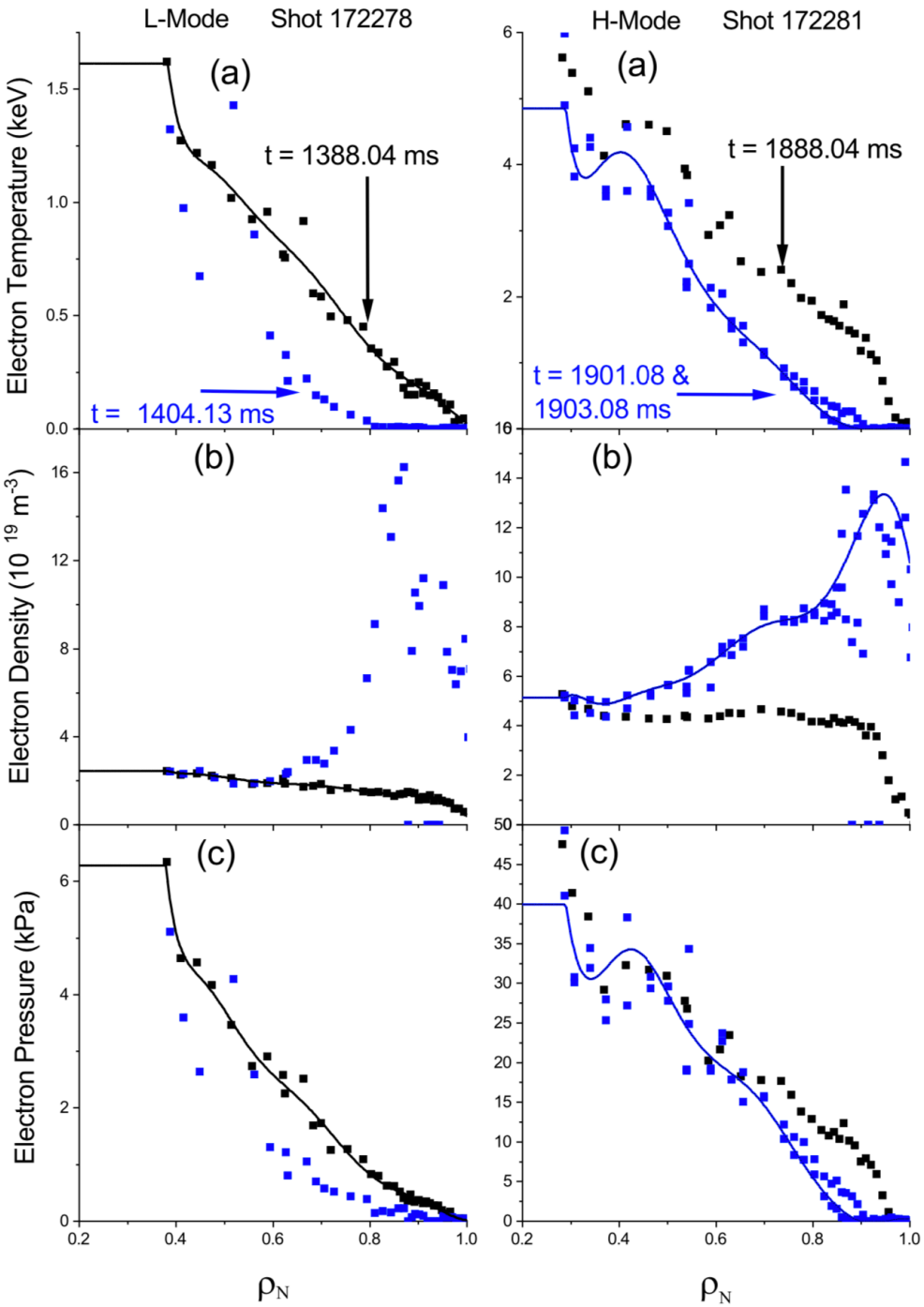

Figure 4: Left - Shot 172278 L-Mode phase. Right - Shot 172281 H-Mode phase. Shown are profiles of (a) electron temperature, (b) electron density, and (c) electron pressure, for the target discharge before it is perturbed by the gas that precedes the SPI fragments, black symbols (at t = 1388.04 ms for the L-mode case) and at t = 1888.04 ms (for the H-mode case) and the corresponding profiles after they are perturbed by the pre-SPI gas, which are shown by the blue symbols. The solid trace shows the actual profile that is used for the simulations described in Section 3. The normalized radius ρ_N is given as the square root of the normalized toroidal flux. The small hollowness the electron temperature profile in discharge 172281 is a consequence of the discharge being perturbed by the pre-SPI gas which starts to enter the plasma at bout 1886 ms.

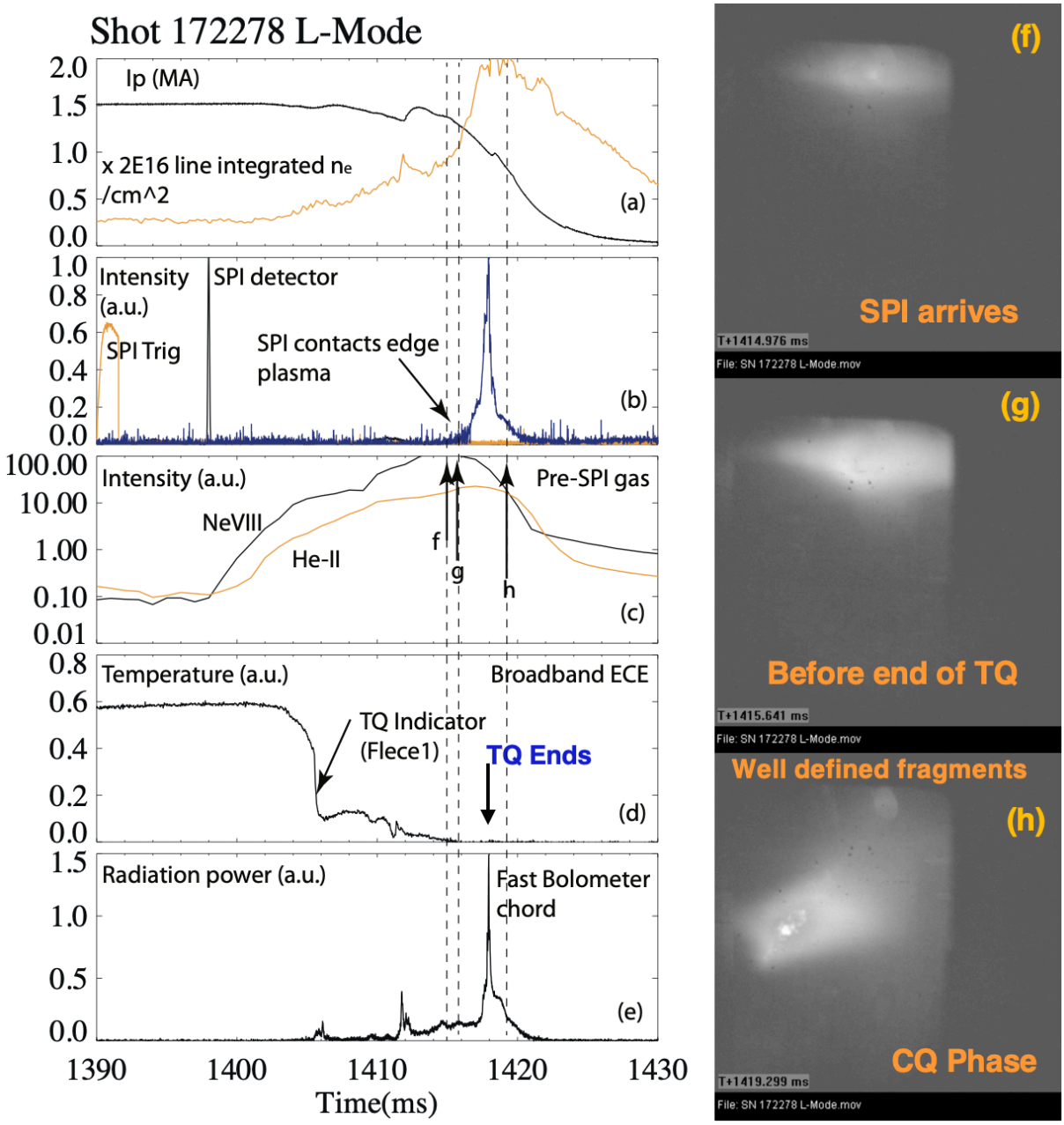

Figure 5: Representative case for injection into a 0.2 MJ low power L-mode discharge that exhibited deep fragment penetration. Shown on the left are: (a) traces corresponding to the plasma current and line integrated electron density, information from the SPI specific diagnostics which shows the SPI trigger time at t=1390ms, signal associated with the transit of the SPI within the injector microwave cavity, labelled as 'SPI detector', and a photodiode signal that records the first interaction of the solid SPI fragments with the edge plasma, (c) time traces of Ne-VIII and He-II spectroscopic signals, (d) a broadband ECE radiometer signal that is indicative of the thermal quench, and (e) signal from a fast bolometer chord that passes through the central region of the plasma. Shown on the right are images from a fast camera diagnostic (corresponding to the view shown in Figure 3): (f) at t = 1414.976 ms when the SPI solid fragments arrive at the plasma edge, (g) at the time corresponding to the thermal quench and current quench phase, and (h) at t= 1419.299 ms a time corresponding to the current quench phase of the discharge. These are for SPI injection into discharge 172278, during the low-power L-mode phase of the discharge. The times corresponding to the camera images are shown on frame (c), as well as by the dashed vertical lines.

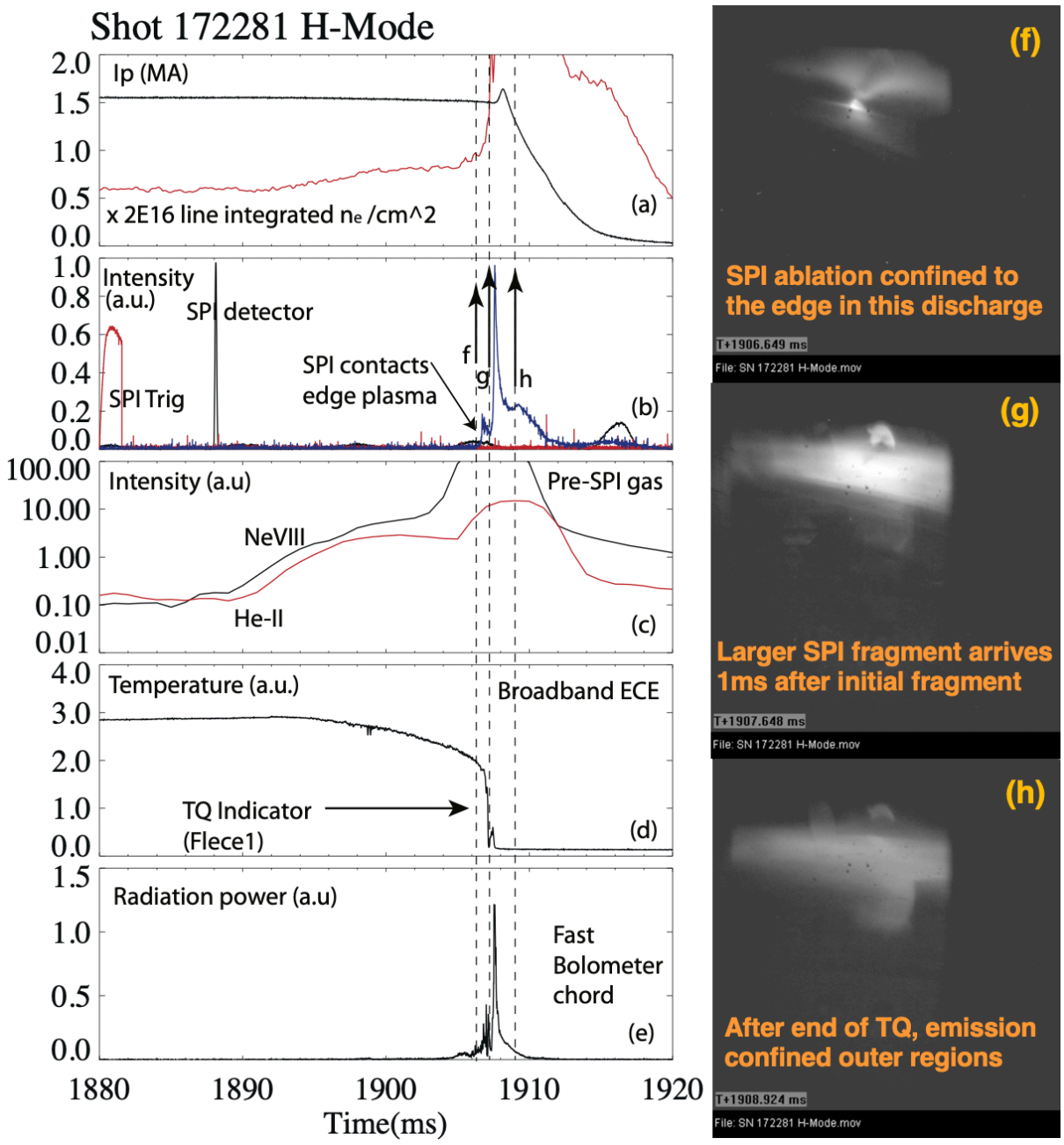

Figure 6: Representative case for injection in to a 2 MJ Super H-Mode discharge that exhibited shallow fragment penetration. Shown on the left are: (a) traces corresponding to the plasma current and line integrated electron density, information from the SPI specific diagnostics which shows the SPI trigger time at t=1880ms, signal associated with the transit of the SPI within the injector microwave cavity, labelled as 'SPI detector', and a photodiode signal that records the first interaction of the solid SPI fragments with the edge plasma, (c) time traces of Ne-VIII and He-II spectroscopic signals, (d) a broadband ECE radiometer signal that is indicative of the thermal quench, and (e) signal from a fast bolometer chord that passes through the central region of the plasma. Shown on the right are images from a fast camera diagnostic (corresponding to the view shown in Figure 3): (f) at t = 1906.649 ms during the start of the thermal quench, (g) at the time corresponding to the end of the thermal quench, and (h) at t= 1908.924 ms a time corresponding to the current quench phase of the discharge. These are for SPI injection into discharge 172281. The times corresponding to the camera images are shown on frame (b), as well as by the dashed vertical lines.

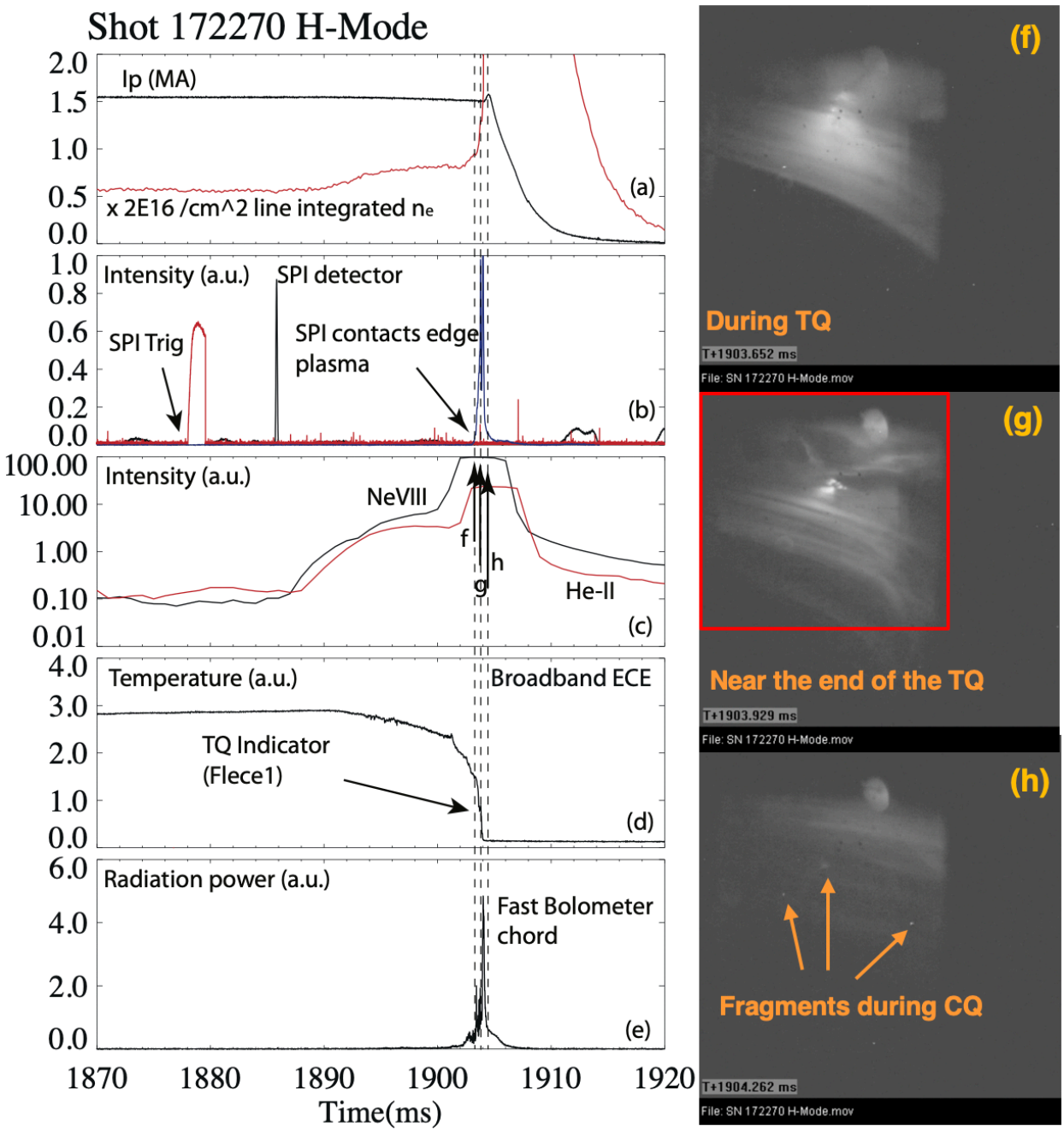

Figure 7: Representative case for injection in to a 2 MJ Super H-Mode discharge that exhibited deep fragment penetration. Shown on the left are: (a) traces corresponding to the plasma current and line integrated electron density, information from the SPI specific diagnostics which shows the SPI trigger time at t=1878 ms, signal associated with the transit of the SPI within the injector microwave cavity, labelled as 'SPI detector', and a photodiode signal that records the first interaction of the solid SPI fragments with the edge plasma, (c) time traces of Ne-VIII and He-II spectroscopic signals, (d) a broadband ECE radiometer signal that is indicative of the thermal quench, and (e) signal from a fast bolometer chord that passes through the central region of the plasma. Shown on the right are images from a fast camera diagnostic (corresponding to the view shown in Figure 3): (f) at t = 1903.652 ms during the thermal quench phase, (g) at the time corresponding to near the end of the thermal quench, and (h) at t= 1904.262 ms a time corresponding to the current quench phase of the discharge. These are for SPI injection into discharge 172270. The times corresponding to the camera images are shown on frame (c), as well as by the dashed vertical lines. The red rectangle in frame (g) is used to compare to the approximate region shown by a similar red rectangle in Figure 8.

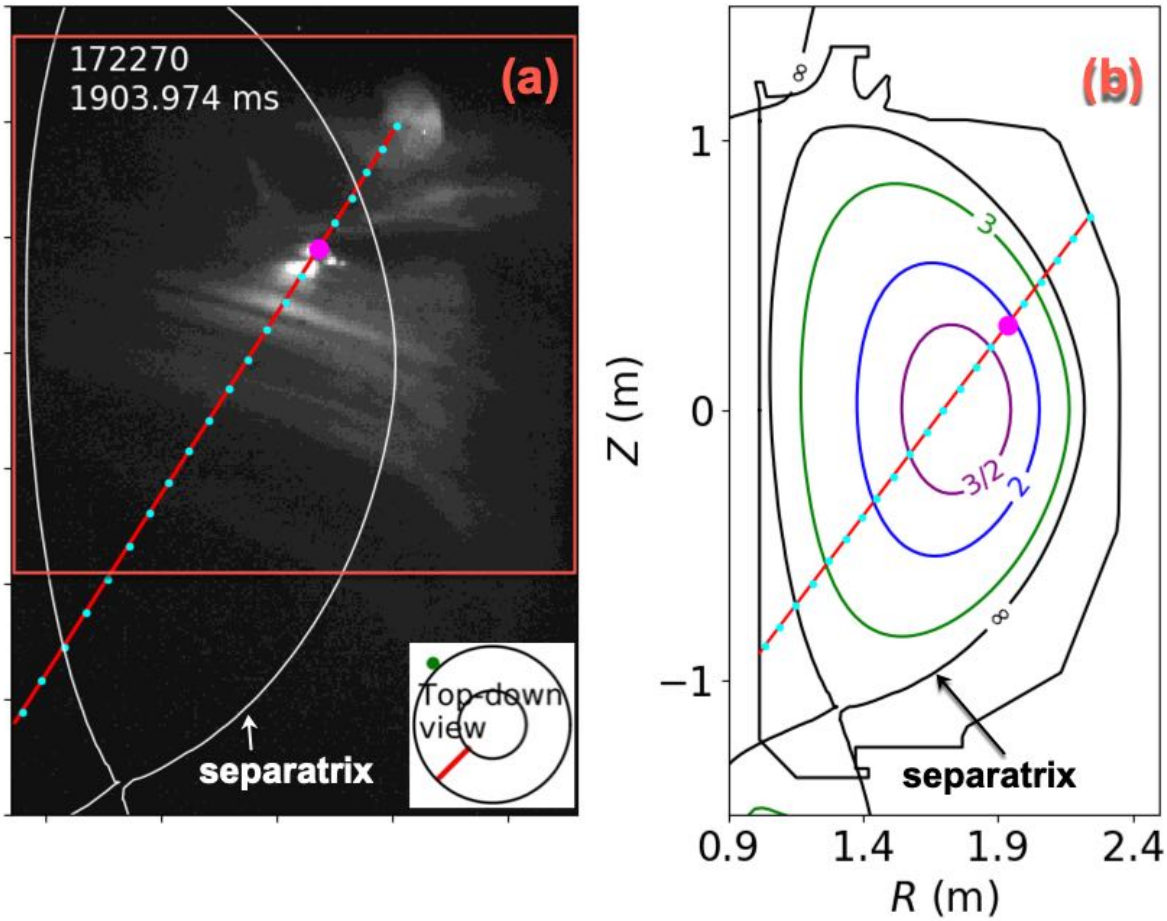

Figure 8: (a) Superimposed on the camera image is a red line that shows the trajectory of the SPI shards. (b) The red trajectory is projected in the R-Z plane and superimposed on an equilibrium reconstruction. The cyan dots along the trajectory in both images are spaced 10 cm apart. The separatrix shown in white on the left frame can be used to compare to the separatrix shown in black on the right frame. The q =3 and q=2 surfaces are also shown. The q=3/2 surface is shown to indicate the proximity of this surface to the q=2 surface. These are for discharge 172270. The red rectangle in the left frame is used to compare to the approximate region shown by the red rectangle in frame (g) in Figure 7.

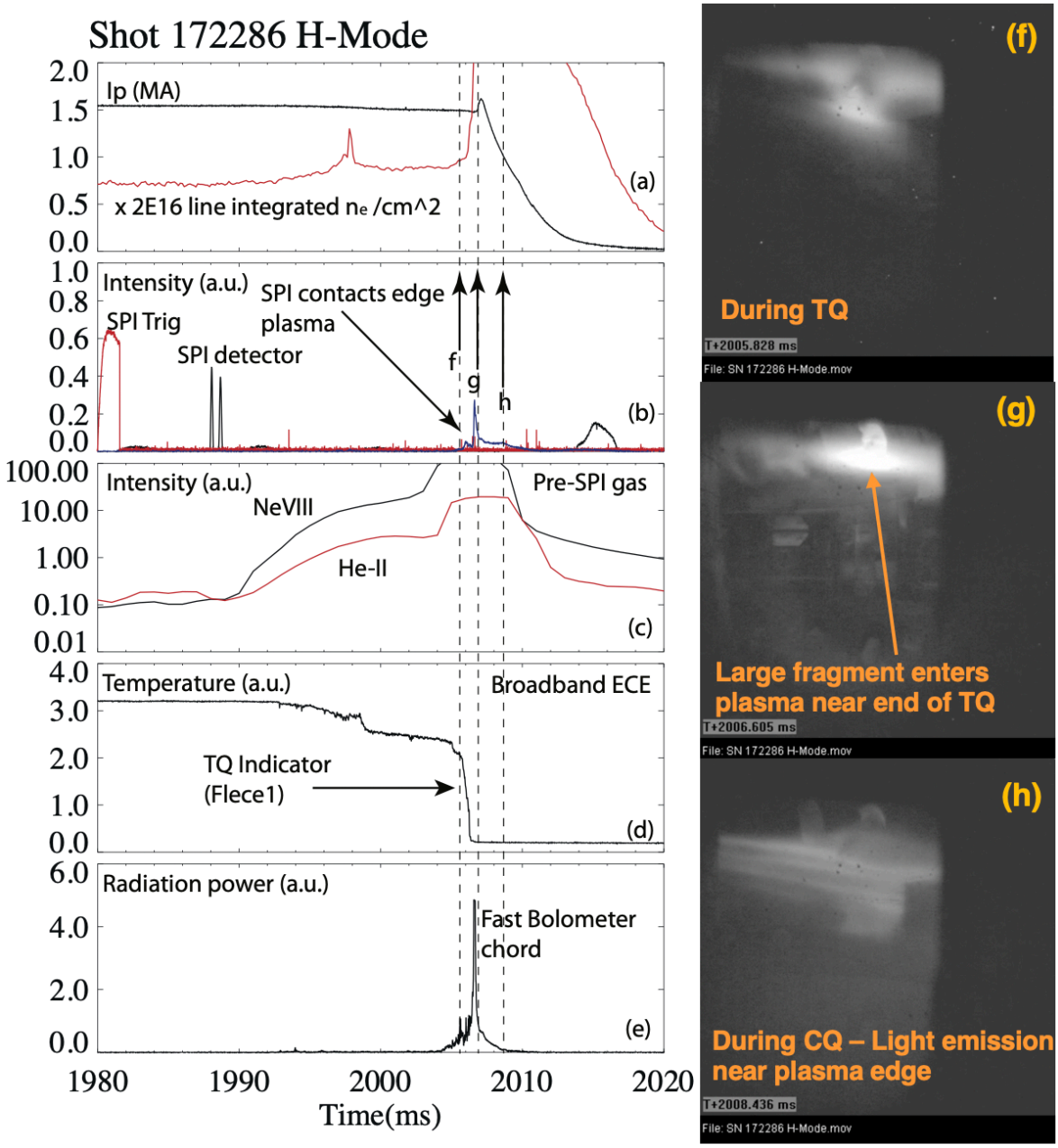

Figure 9: Representative case for injection in to a 2.2 MJ Super H-Mode discharge that exhibited shallow fragment penetration and the pellet breaking into two pieces within the acceleration region. Shown on the left are: (a) traces corresponding to the plasma current and line integrated electron density, information from the SPI specific diagnostics which shows the SPI trigger time at t=1980 ms, signal associated with the transit of the SPI within the injector microwave cavity, labelled as 'SPI detector', and a photodiode signal that records the first interaction of the solid SPI fragments with the edge plasma, (c) time traces of Ne-VIII and He-II spectroscopic signals, (d) a broadband ECE radiometer signal that is indicative of the thermal quench, and (e) signal from a fast bolometer chord that passes through the central region of the plasma. Shown on the right are images from a fast camera diagnostic (corresponding to the view shown in Figure 3): (f) at t = 2005.828 ms during the thermal quench phase, (g) at the time corresponding to near the end of the thermal quench, and (h) at t= 2008.436 ms a time corresponding to the current quench phase of the discharge. These are for SPI injection into discharge 172286. The times corresponding to the camera images are shown on frame (b), as well as by the dashed vertical lines.

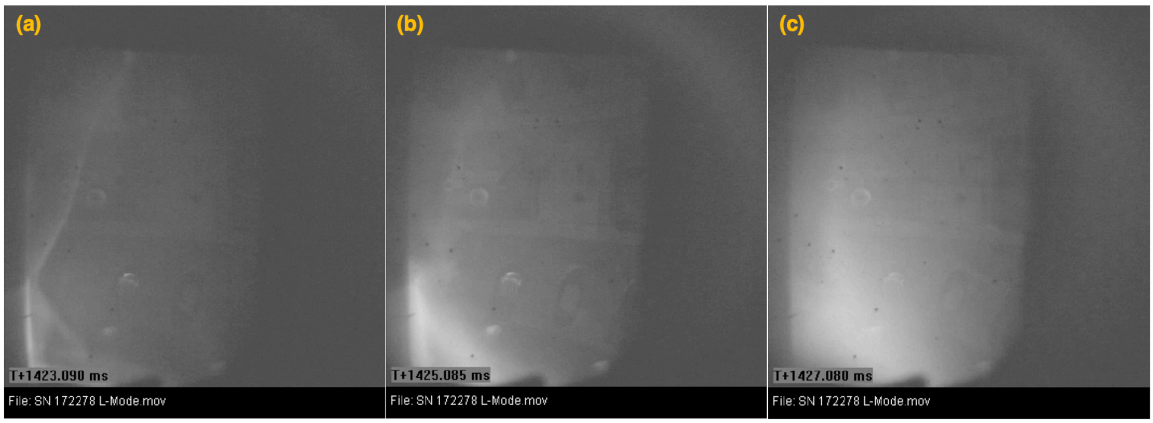

Figure 10: Fast camera images from discharge 172278 showing SPI fragments impacting the inner wall (frame a at 1423.09 ms) and then the neon cloud propagating back into the plasma (frames b at 1425.08 ms and frame c at 1427.08 ms).

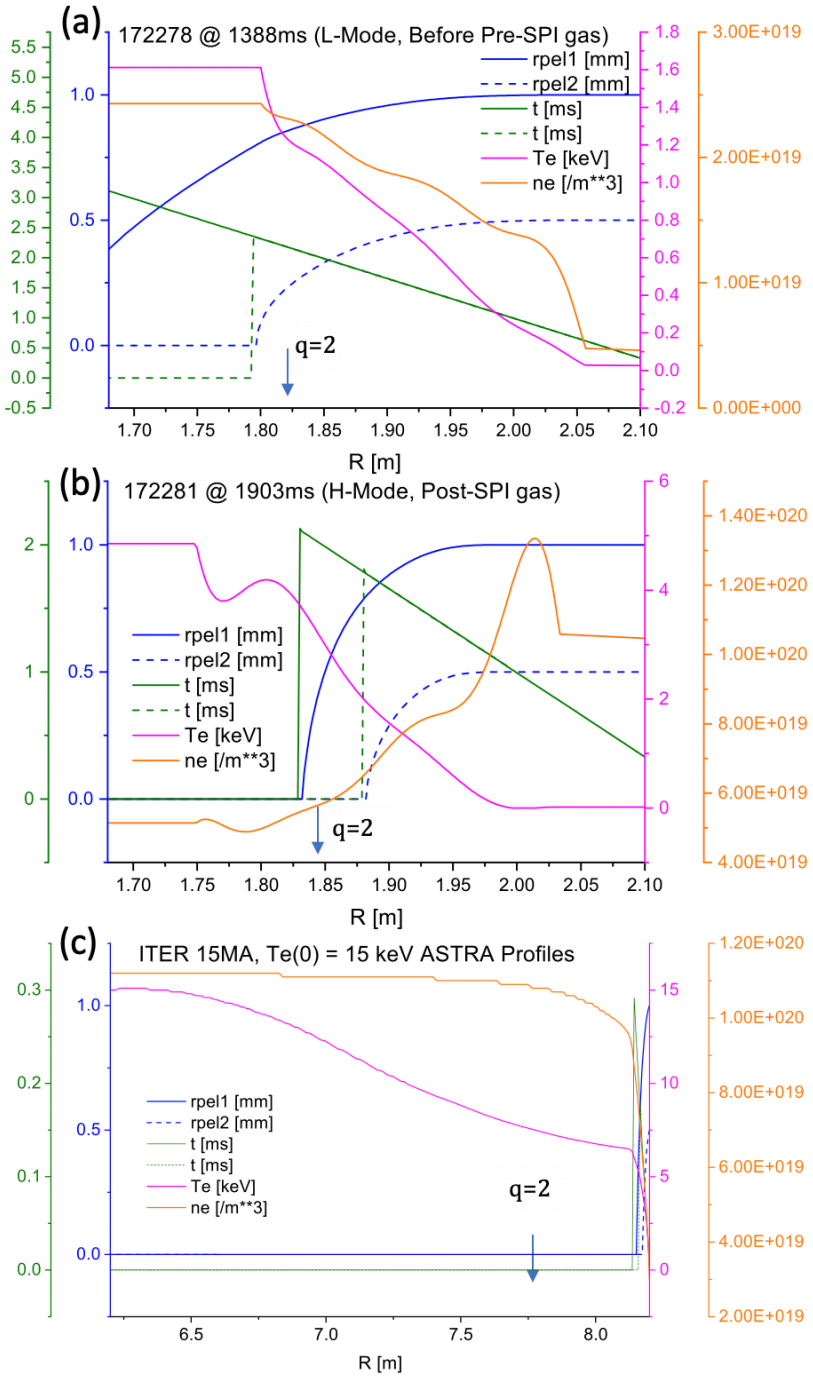

Figure 11: Calculations of single neon pellet penetration into discharges corresponding to those representative of the low-power L-mode case (0.2 MJ), the H-mode case (1.6 MJ), and for a 350 MJ ITER H-mode discharge, with Te(0) = 15 keV. Note that the electron temperature and density profiles for 172281 (frame b) use profiles that are the result of cooling by the pre-SPI gas but for the low-power L-mode (frame a) the profiles before the arrival of the pre-SPI gas are used. Calculations are carried out for 2 mm and 1 mm diameter neon pellet with an injection velocity of 200 m/s. The green solid trace is a plot of the propagation time vs. distance for the 2 mm pellet. In frame (b) it shows that the 2 mm pellet is fully ablated in about 2 ms. The green dashed trace is for the propagation time vs. distance for the 1 mm pellet. Note that these do not simulate SPI injection, during which many fragments are injected. The DIII-D cases use the same

injection angle as that in the experiment. The ITER cases assumes pure radial injection from the vessel mid-plane. The approximate location of the q=2 surface is indicated by the blue arrow.

References

[1] Whyte, D.G., Evans, T.E., Kellman, A.G., *et al* 1997 Energy balance, radiation and stability during rapid plasma termination via impurity pellet injections on DIII-D, General Atomics Technical Report No. GA-A22639

[2] Finken K.H., Lehnen M. and Bozhenkov S.A. 2008 Gas flow analysis of a disruption mitigation valve (DMV), Nucl. Fusion **48** 115001

[3] Bozhenkov S.A., Finken K.H., Lehnen M. and Wolf R.C. 2007 Main characteristics of the fast disruption mitigation valve, Rev. Sci. Instrum. **78** 033503

[4] Hollmann E.M. *et al* 2015 Status of research toward the ITER disruption mitigation system, Phys. Plasmas **22** 021802

[5] Whyte D.G. *et al* 2003 Disruption mitigation with high pressure noble gas injection, J. Nucl. Mater. **313–6** 1240

[6] Pautasso G. *et al* 2009 Disruption studies in ASDEX Upgrade in view of ITER, Plasma Phys. Control. Fusion **51** 124056

[7] Granetz R.S. *et al* 2007 Disruption mitigation studies on ALCATOR C-MOD and DIII-D, Nucl. Fusion **47** 1086

[8] Reux C. *et al* 2010 Experimental study of disruption mitigation using massive injection of noble gases on Tore Supra, Nucl. Fusion **50** 095006

[9] Lehnen, M. *et al* 2015 Disruptions in ITER and strategies for their control and mitigation, Journal Nuclear Materials **463** 39-48

[10] Leonov V. *et al* 2014 Simulation of the pre-thermal quench stage of disruptions during massive gas injection and projections for ITER Proc. IAEA-FEC 2014 Conf.
(St. Petersburg, Russia, 13–18 October) TH/P3-35 (www-naweb.iaea.org/napc/physics/FEC/FEC2014/fec2014- preprints/478_THP335.pdf)

[11] Commaux N. *et al* 2016 First demonstration of rapid shutdown using neon shattered pellet injection for thermal quench mitigation on DIII-D, Nucl. Fusion **56** 046007

[12] Baylor, L.R. *et al* 2019 Shattered pellet injection technology design and characterization for disruption mitigation experiments, Nucl. Fusion **59** 066008

[13] Herfindal, J.L. *et al* 2019 Injection of multiple shattered pellets for disruption mitigation in DIII-D, Nucl. Fusion **59** 106034

[14] Baylor L.R. *et al* 2010 Disruption mitigation technology concepts and implications for ITER, IEEE Trans. Plasma Sci. **38** 419

[15] Li, Y. *et al* 2018 Design of a shattered pellet injection system on J-TEXT tokamak, Rev. Sci. Instrum. **89** 10K116

[16] Snyder, P.B., Solomon, W. M., Burrell, K. H. *et al* 2015 Super H-mode: theoretical prediction and initial observations of a new high performance regime for tokamak operation, Nucl. Fusion **55** 083026.

[17] Parail, A., Albanese, R., Ambrosino, R. *et al* 2013 Self-consistent simulation of plasma scenarios for ITER using a combination of 1.5D transport codes and free-boundary equilibrium codes, Nucl. Fusion **53** 113002

[18] Casper, T., Gribov, Y., Kavin, A *et al* 2014 Development of the ITER baseline inductive scenario, Nucl. Fusion **54** 013005

[19] Izzo, V.A., and Parks, P.B. 2017 Modeling of rapid shutdown in the DIII-D tokamak by core deposition of high-Z material, Phys. Plasmas **24** 060705

[20] Ferraro N.M., Lyons, B.C., Kim, C.C. *et al* 2019 3D two-temperature magnetohydrodynamic modeling of fast thermal quenches due to injected impurities in tokamaks, Nucl. Fusion **59** 016001

[21] Samulyak, R., Lu, T., Parks, P., 2007 A magnetohydrodynamic simulation of pellet ablation in the electrostatic approximation, Nucl. Fusion **47** Vol 2, 103

[22] Wang, X., Samulyak, R., Jiao, X., Yu, K., 2016 AP-Cloud: Adaptive particle-in-cloud method for optimal solutions to Vlasov-Poisson equation, Journal of Computational Physics **316**, 682-699

[23] Kuteev B.V., Sergeev V. Yu., Sudo S., 1995 Emergency discharge quench or rampdown by a noble gas pellet, Nucl. Fusion **35** 1167

[24] Shiraki D. *et al* 2016 Thermal quench mitigation and current quench control by injection of mixed species shattered pellets in DIII-D, Phys. Plasmas **23** 0625516

[25] Austin, M.E. and Lohr, J. 2003 Electron cyclotron emission radiometer upgrade on the DIII-D tokamak, Rev. Sci. Instrum. **74**, 1457

[26] Hollmann, E.M., Jernigan, T.C., Groth, M. *et al* 2005 Measurements of impurity and heat dynamics during noble gas jet-initiated fast plasma shutdown for disruption mitigation in DIII-D, Nucl. Fusion **45** 1046

[27] Whyte, D.G. *et al* 1998 Rapid inward impurity transport during impurity pellet injection on the DIII-D tokamak, Phys. Rev. Lett. **81**, 4392

[28] Hu., D., Nardon, E., Lehnen, M. *et al* 2018 3D non-linear MHD simulation of the MHD response and density as a result of shattered pellet injection, Nucl. Fusion **58** 126025

[29] Houlberg W.A., Milora S. L., Attenberger S. E., 1998 Neutral and plasma shielding model for pellet ablation, Nucl. Fusion **28** 595

[30] Baylor L. 2017 Developments in shattered pellet technology and implementation on JET and ITER, *PPPL TSD Workshop Report* Princeton Plasma Physics Laboratory (http://tsdw. pppl.gov/Talks/2017/Lexar/Monday%20Session%201/ Baylor.pdf)

[31] Polevoi, A.R., Campbell, D.J., Chuyanov, A.A. *et al* 2013 Assessment of plasma parameters for the low activation phase of ITER operation, Nucl. Fusion **53** 123026

[32] Izzo, V.A., Parks, P.B., Lao, L.L. 2009 DIII-D and ITER rapid shutdown with radially uniform deuterium delivery, Plasma Physics and Controlled Fusion **51** 105004

[33] Izzo, V.A. 2006 A Numerical Investigation of the Effects of Impurity Penetration Depth on Disruption Mitigation by Massive High-Pressure Gas Jet, Nucl. Fusion **46**, 541

[34] Hollmann, E.M. *et al* 2013 Characterization of Heat Loads from Mitigated and Unmitigated Vertical Displacement Events in DIII-D, Phys. Plasmas **20**, 062501